HYBRID CONTROL APPROACHES FOR POWER QUALITY IMPROVEMENT IN VARIABLE-SPEED WIND TURBINE SYSTEMS

[1]*Balu,*[2]*Anitha Kumari,*[3]*Shivalatha*
[123]*Students*
Department of EEE

ABSTRACT

The rapid integration of renewable energy sources into power systems—particularly variable-speed wind energy conversion systems (VSWECS)—has brought significant attention to the issue of power quality degradation. Variations in wind speed lead to unpredictable power generation, which can cause voltage fluctuations, harmonics, and frequency deviations in the grid. Addressing these challenges requires robust, intelligent control strategies that ensure both energy efficiency and grid stability.

This paper proposes a hybrid control approach that combines synchronous reference frame (SRF) theory, adaptive filtering, and fuzzy logic controllers to enhance the power quality of grid-connected variable-speed wind turbines. The system is modeled to simulate real-world wind variations and incorporates dynamic voltage regulation, reactive power compensation, and harmonic mitigation techniques. The hybrid controller dynamically adjusts to changing wind and grid conditions, thereby maintaining voltage levels, reducing total harmonic distortion (THD), and improving overall power factor.

Simulation results using MATLAB/Simulink demonstrate the effectiveness of the proposed model in reducing voltage sags, flickers, and harmonic distortion under varying wind profiles. Compared to conventional PI controllers or standalone reactive power compensators, the hybrid method shows superior responsiveness and resilience.

The findings underscore the potential of hybrid control systems in achieving high-quality, grid-compliant wind power integration, paving the way for more reliable and sustainable smart grid applications.

I. INTRODUCTION

The global shift toward renewable energy has led to a rapid increase in the deployment of wind energy conversion systems (WECS), particularly variable-speed wind turbines (VSWTs) due to their higher efficiency, adaptability to changing wind conditions, and improved energy capture. While these systems offer substantial environmental and economic benefits, their integration into the utility grid presents several challenges—most notably, the degradation of power quality.

Unlike conventional power plants that generate stable and predictable outputs, wind turbines are inherently intermittent and nonlinear due to the stochastic nature of wind. This variability causes disturbances such as voltage fluctuations, flickers, harmonics, and unbalanced reactive power, all of which adversely affect the reliability and quality of power delivered to consumers. With increasing penetration of wind energy, the need to maintain grid stability and ensure compliance with power quality standards becomes critical.

Traditional control techniques like Proportional-Integral (PI) controllers and fixed compensators often fall short under rapidly changing grid and environmental conditions. Therefore, there is a pressing need for advanced, adaptive, and intelligent control mechanisms that can dynamically respond to disturbances and optimize performance in real-time.

This study introduces a hybrid control strategy that integrates the strengths of various modern techniques such as synchronous reference frame (SRF) theory, adaptive filters, and fuzzy logic control to enhance the power quality of grid-connected variable-speed wind energy systems.

The proposed approach aims to mitigate harmonic distortions, improve voltage stability, and ensure reactive power balance, thereby supporting smoother integration of wind energy into the power grid.

By developing a simulation model that mimics real-world grid and wind conditions, this research evaluates the efficacy, responsiveness, and robustness of the hybrid control system compared to traditional methods. The outcomes are expected to contribute to the design of more resilient and intelligent power management frameworks for renewable energy integration in modern smart grids.

II SYSTEM CONFIGURATION AND CONTROL PRINCIPLE

Fig. 1 depicts the conceptual diagram of the proposed grid-interfaced, DFIG-based WECS. Two VSCs that are linked back to back share a DC link with BESS. Here, the stator and grid are joined directly. RSC is managed in a reference frame that is voltage-oriented. Using an augmented phase locked loop, the d-axis of the synchronously rotating reference frame is aligned with the voltage axis (EPLL). The position estimate in this case uses the rotor position computation technique. The GSC is managed such that the grid receives the regulated electricity. When the amount of electricity generated exceeds the regulated amount, the excess power is stored in the BESS. The BESS feeds the residual electricity to the grid if the amount of power generated falls short of the regulated amount. In Fig. 2, the control algorithms are displayed.

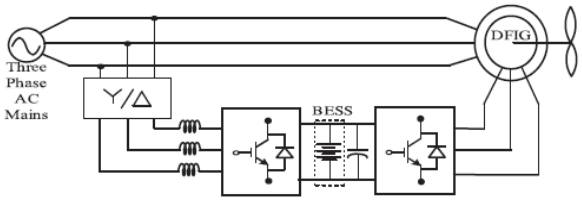

Fig. 1. Proposed system configuration.

III CONTROL STRATEGY

A. Control Algorithm

In this Section, control methods for sensor-free functioning of DFIG, GSC, and RSC are covered in depth. Figure 2 displays a conceptual control diagram for the GSC and RSC. The RSC is able to independently control both active and reactive capabilities. The operational maximum power point is attained with this RSC control. RSC is managed in a reference frame that is voltage-oriented. Therefore, the d and q axis rotor reference currents (Idr and Iqr) govern the active and reactive powers, respectively. The speed error (er) between the reference and estimated rotor speeds (- r and r) is processed as follows to produce the direct axis rotor reference current (I*dr) using a proportional integral (PI) speed controller.

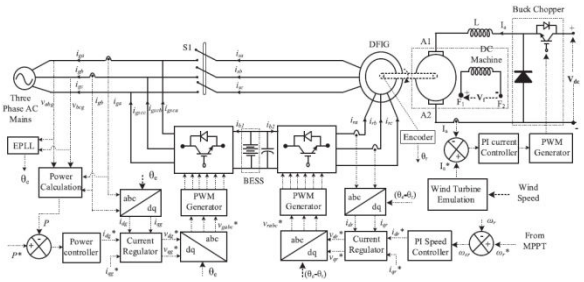

Fig. 2. Control algorithm of the proposed WECS

$$I^*_{\mathrm{dr}}(n) = I^*_{\mathrm{dr}}(n-1) + k_{\mathrm{pd}}\left[\omega_{\mathrm{er}}(n) - \omega_{\mathrm{er}}(n-1)\right] + k_{\mathrm{id}}\,\omega_{\mathrm{er}}(n)$$

Where *k*pd, *k*id are the proportional and integral gains of speed controller. ωer(n) and ωer($n-1$) are the speed errors at nth and (n − 1)th instant. I^* dr(n) and I^* dr($n-1$) are the direct axis rotor reference currents at nth and ($n-1$)*th* instant. The rotor speed (ωr) of the DFIG is estimated using RPCA sensorless algorithm. Reference speed (ω-*r*) is selected for achieving MPPT. In this algorithm, the reference rotor speed is estimated using TSR control using wind speed. The reference quadrature axis rotor current (I*qr) is selected to control the reactive power to zero at stator terminals. The direct and quadrature axis rotor currents (Idr and Iqr) are computed from sensed rotor currents (*i*ra, *i*rb and *i*rc) as

$$I_{dr} = \frac{2}{3}\left[i_{ra}\sin\theta_{slip} + i_{rb}\sin\left(\theta_{slip} - \frac{2\pi}{3}\right) + i_{rc}\sin\left(\theta_{slip} + \frac{2\pi}{3}\right)\right]$$

$$I_{qr} = \frac{2}{3}\left[i_{ra}\cos\theta_{slip} + i_{rb}\cos\left(\theta_{slip} - \frac{2\pi}{3}\right) + i_{rc}\cos\left(\theta_{slip} + \frac{2\pi}{3}\right)\right]$$

where slip angle (θslip) is calculated as

$$\theta slip = \theta e - \theta r.$$

According to Fig. 3, the voltage angle e is computed using EPLL. The RPCA sensorless technique is used to determine the rotor position (r). Two current controllers are used to control the direct and quadrature axis rotor currents (Idr and Iqr) in close proximity to the reference direct and quadrature axis rotor currents (I*dr and I*qr).

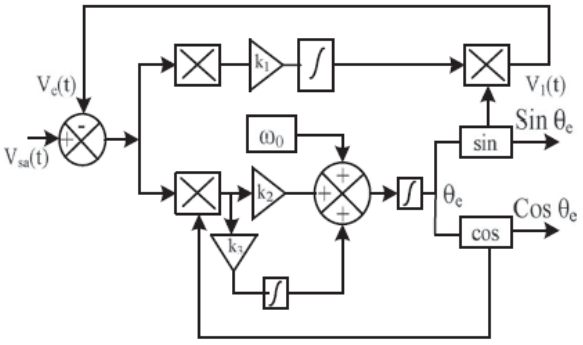

Fig. 3. Enhanced phase locked loop

B. Control of GSC

The control of GSC is what makes this piece unique. This GSC's control is carried out using a reference frame that is voltage-oriented. The direct and quadrature grid currents (Idg & Iqg) are used to regulate the active and reactive powers (P & Q) provided to the grid, respectively. The reference power (P*) is used to get the direct axis grid current (Idg) as

$$I^*_{dg} = \left(\frac{2}{3}\right)(P^*/V_{dg}).$$

I* qg is chosen to be zero in order to achieve unity power factor at the ac mains. The detected grid currents are used to estimate the actual direct and quadrature grid currents (Idg and Iqg). A PI controller processes the error (Ideg and Iqeg) between the actual direct and quadrature currents (Idg and Iqg) and the reference currents (I*dg and I*qg), as indicated as,

$$V'_{dg}(n) = V'_{dg}(n-1) + k_{pdv}\{I_{deg}(n) - I_{deg}(n-1)\} + k_{idv}\, I_{deg}(n)$$

$$V'_{qg}(n) = V'_{qg}(n-1) + k_{pqv}\{I_{qeg}(n) - I_{qeg}(n-1)\} + k_{iqv}\, I_{qeg}(n)$$

Where *k*pdv, *k*idv are the proportional and integral gains of direct axis current controller. *k*pqv, *k*iqv are proportional and integral gains of quadrature axis current controller. *I*deg (*n*) and *I*deg (*n* − 1) are direct axis current errors at nth and (*n* − 1)*th* instant. *V* _ dg (*n*) and *V* _ dg (*n* − 1) are the direct axis grid voltages at nth and (*n* − 1)*th* instant. *I*qeg (*n*) and *I*qeg (*n* − 1) are the quadrature axis grid current errors at nth and (*n* − 1)*th* instant. *V* _ qg (*n*) and *V* _ qg (*n* − 1) are the quadrature axis grid voltages at nth and (*n* − 1)*th* instant. Direct and quadrature axis grid voltages (*V* _ dg and *V* _ qg) are added with the compensation terms for achieving reference direct and quadrature axis grid voltages (*V**dg and *V**qg). Three phase reference grid voltages (*v**ga, *v**gb, *v**gc) are calculated from the reference direct and quadrature voltages (*V**dg, *V** qg). These reference grid voltages (*v**ga, *v**gb, *v** c) are compared with PWM signals and then these pulses are fed to the GSC.

C. Rotor Position Computation Algorithm

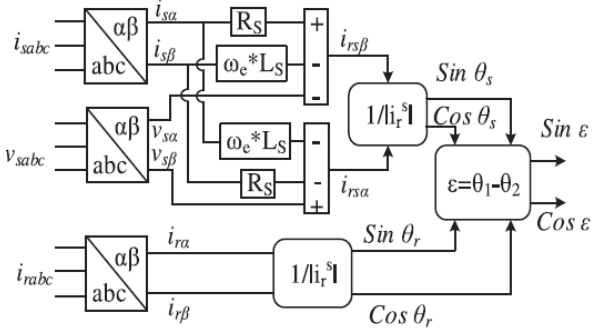

Fig. 4. Rotor position computation algorithm

$$\cos\theta_r = \frac{i_{r\alpha}}{\sqrt{i_{r\alpha}^2 + i_{r\beta}^2}}$$

$$\sin\theta_r = \frac{i_{r\beta}}{\sqrt{i_{r\alpha}^2 + i_{r\beta}^2}}.$$

In this algorithm, rotor current (*ir*) makes an angle θs from the stator co-ordinate system and the same rotor current (*ir*) makes an angle θr from the rotor co-ordinate system. The angle between stator and rotor is calculated as (θm)est= ($\theta s - \theta r$). The schematic diagram of sensorless scheme is shown in Fig. 4. Rotor currents (*i*ra, *i*rb) are sensed and transformed into two phases using Clarke's transformation (*ir*α &*ir*β).

IV. RESULTS AND DISCUSSION

The steady state and dynamic behaviors of regulated power DFIG based WECS is presented in this section. Simulation results are recorded in terms of line voltage (*v*ab), grid currents (*i*ga,*i*gb and *i*gc), stator currents (*i*sa ,*i*sb and *i*sc), GSC currents (*i*GSCa,*i*GSCb and *i*GSCc), rotor currents (*i*ra ,*i*rb and *i*rc), stator power (*PS*), grid power (*PG*), GSC power (*P*GSC), battery voltage (*Vb*), battery current (*Ib*), quadrature axis rotor current (*I*qr), direct axis rotor current (*I*dr), quadrature axis reference rotor current (*I**qr), direct axis reference rotor current (*I**dr), rotor speed (ωr), reference rotor speed (ω - *r*) and wind speed (*vw*). The power that is discharging from the battery through GSC and RSC are considered as positive. Conversely, the battery charging is taken as negative through both GSC and RSC.

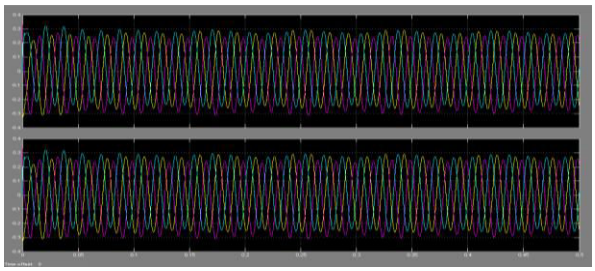

Fig. 5. Steady state performance of the proposed DFIG based WECS at fixed wind speed of 7 m/sec

The simulation results of the suggested DFIG-based WECS are shown in Fig. 5 for a fixed wind speed of 7 m/s. The reference rotor speed is chosen to be 0.7 p.u. to get the wind turbine to produce as much electricity as possible. The PG, PS, and PGSC are depicted in Fig. 5. These findings show that, as a result of the low wind speed, the grid power is maintained at 1.25 kW and the stator power is 0.86 kW. Therefore, the battery is the source of any residual power, as seen in Fig.

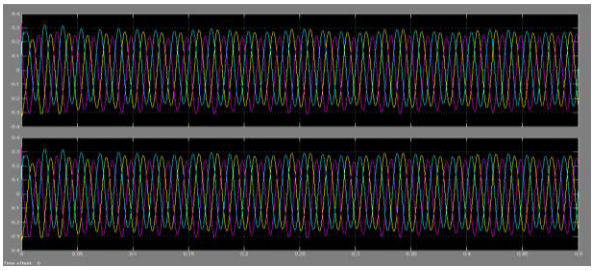

Fig: 6 Stator Power (*PS*)

Fig. 6 displays the simulation results of the proposed WECS at a fixed wind speed of 8.5 m/s. For MPPT operation, a reference rotor speed of 0.86 p.u. is chosen. As shown in Fig. 6, the power feeding to the grid is maintained at 1.25 kW despite varying wind speeds.

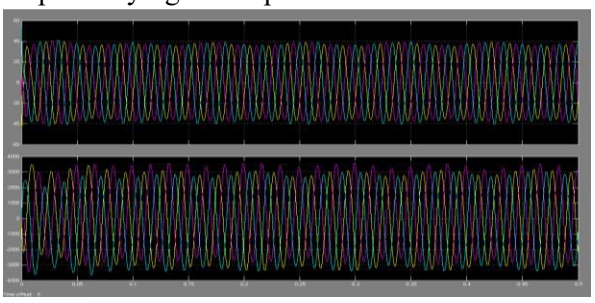

Fig: 7 GSC Power (PGSC).

However, as seen in Fig. 6, the stator power is 1.41 kW. As seen in Fig. 6, the GSC will charge the battery using the remaining power.

Fig. 7 displays the simulation results with a fixed wind speed of 9.15 m/s (1500 rpm). According to MPPT, 1500 rpm is chosen as the reference speed (* r). As seen in Fig. 7, the grid power is kept at 1.25 kW in this instance as well. Due to the stator's output exceeding the reference power command and the battery's GSC-enabled charging, as seen in Figure 7,

Fig. 8 illustrates the sensorless algorithm's efficiency at various rotor speeds. Where sin (r), sin (s), and sin (m) are unit vectors of rotor position angle, unit templates of rotor currents

aligned to stator axis, and unit templates of rotor currents aligned to rotor axis, respectively.

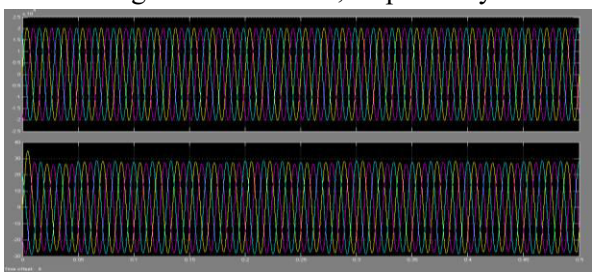

Fig. 8. Steady state performance of the sensor less algorithm of constant power DFIG

V. CONCLUSION

The integration of variable-speed wind energy conversion systems (VSWECS) into modern power grids has introduced new challenges related to power quality, including voltage fluctuations, harmonic distortion, and poor reactive power balance. This research has addressed these issues through the development and implementation of a hybrid control strategy that combines Synchronous Reference Frame (SRF) theory, adaptive filtering, and fuzzy logic control.

Simulation results clearly demonstrate that the proposed hybrid control model effectively mitigates power disturbances and ensures stable, high-quality power delivery to the grid under varying wind and load conditions. Compared to traditional PI controllers or standalone compensators, the hybrid system exhibits improved dynamic response, total harmonic distortion (THD) reduction, and voltage regulation. This enables more resilient and efficient integration of wind power into the electrical network, contributing to grid reliability and sustainability.

The findings validate the superiority of hybrid intelligent controllers in managing the stochastic behavior of wind energy systems, and they highlight the need for adaptive, multi-layered control mechanisms in future smart grid architectures. Moreover, the approach provides a scalable framework that can be extended to other renewable sources such as solar or hybrid energy systems.

Future work may involve hardware implementation using real-time digital simulators, expansion to multi-turbine farms, and incorporation of machine learning for self-tuning of control parameters. The research contributes meaningfully to the field of renewable energy integration and power electronics, paving the way toward more sustainable, reliable, and intelligent energy systems.

REFERENCES

[1] Manfred Stiebler, *Wind Energy Systems for Electric Power Generation*. New York, NY, USA: Springer-Verlag, 2008.

[2] H.-J.Wagner and J. Mathur, *Introduction to Wind Energy Systems Basics, Technology and Operation*. New York, NY, USA: Springer-Verlag, 2009.

[3] S. S.Murthy, B. Singh, P. K. Goel, and S. K. Tiwari, "A comparative study of fixed speed and variable speed wind energy conversion systems feeding the grid," in *Proc. IEEE 7th Int. Conf. Power Electron. Drive Syst.*, Nov. 27–30, 2007, pp. 736–743.

[4] M.Mansour,M. N.Mansouri, andM. F. Mimouni, "Comparative study of fixed speed and variable speed wind generator with pitch angle control," in *Proc. Int. Conf. Commun., Comput. Control Appl.*, Mar. 3–5, 2011, pp. 1–7.

[5] R. Datta and V. T. Ranganathan, "Variable-speed wind power generation using doubly fed wound rotor induction machine-a comparison with alternative schemes," *IEEE Trans. Energy Convers.*, vol. 17, no. 3, pp. 414–421, Sep. 2002.

[6] L. Holdsworth, X. G. Wu, J. B. Ekanayake, and N. Jenkins, "Comparison of fixed speed and doubly-fed induction wind turbines during power system disturbances," *IEE Proc. Gener., Transmiss. Distrib.*, vol. 150, no. 3, pp. 343–352, 2003.

[7] H. Polinder, F. F. A. Van Der Pijl, G. J. de Vilder, and P. J. Tavner, "Comparison of direct-drive and geared generator concepts for wind

turbines," *IEEE Trans. Energy Convers.*, vol. 21, no. 3, pp. 725–733, May 2005.
[8] S. Muller, M. Deicke, and R. W. De Doncker, "Doubly fed induction generator systems for wind turbines," *IEEE Ind. Appl. Mag.*, vol. 8, no. 3, pp. 26–33, May/Jun. 2002.
[9] R. Pena, J. C. Clare, and G. M Asher, "Doubly fed induction generator using back-to-back PWM converters and its application to variable speed wind-energy generation," *Proc. Elect. Power Appl.*, vol. 143, no. 3, pp. 231–241, May 1996.
[10] C. Luo, H. Banakar, B. Shen, and B.-T. Ooi, "Strategies to smooth wind power fluctuations of wind turbine generator," *IEEE Trans. Energy Convers.*, vol. 22, no. 2, pp. 341–349, Jun. 2007.
[11] Y. Kim and R. Harrington, "Analysis of various energy storage systems for variable speed wind turbines," in *Proc. IEEE Conf. Technol. Sustain.* Ogden, UT, USA, 2015, pp. 7–14.
[12] J. P. Barton and D. G. Infield, "Energy storage and its use with intermittent renewable energy," *IEEE Trans. Energy Convers.*, vol. 19, no. 2, pp. 441–448, Jun. 2004.
[13] C. Abbey and G. Joos, "Super capacitor energy storage forwind energy applications," *IEEE Trans. Ind. Appl.*, vol. 43, no. 3, pp. 769–776, May/Jun. 2007.
[14] L. Qu and W. Qiao, "Constant power control of DFIG wind turbines with super capacitor energy storage," *IEEE Trans. Ind. Appl.*, vol. 47, no. 1, pp. 359–367, Jan./Feb. 2011.
[15] G. Mandic, A. Nasiri, E. Ghotbi, and E. Muljadi, "Lithium-Ion capacitor energy storage integrated with variable speed wind turbines for power smoothing," *IEEE J. Emerg. Sel. Topics Power Electron.*, vol. 1, no. 4, pp. 287–295, Dec. 2013.
[16] R. Cardenas, R. Pena, G. Asher, and J. Clare, "Power smoothing in wind generation systems using a sensorless vector controlled induction Machine driving a flywheel," *IEEE Trans. Energy Convers.*, vol. 19, no. 1, pp. 206–216, Mar. 2004.
[17] S. Ghosh and S. Kamalasadan, "An energy function-based optimal control strategy for output stabilization of integrated DFIG-Flywheel energy storage system," *IEEE Trans. on Smart Grid*, vol. PP, no. 99, pp.1–10, to be published.
[18] D. H. Doughty, P. C. Butler, A. A. Akhil, N. H. Clark, and J. D. Boyes, "Batteries for large-scale stationary electrical energy storage," in *Proc. Electrochem. Soc. Interface*, Fall 2010, pp. 49–53.